NOTES AND CORRESPONDENCE

El Niño Modoki Impacts on Australian Rainfall

ANDRÉA S. TASCHETTO AND MATTHEW H. ENGLAND

Climate Change Research Centre, University of New South Wales, Sydney, New South Wales, Australia

(Manuscript received 15 April 2008, in final form 27 November 2008)

ABSTRACT

This study investigates interseasonal and interevent variations in the impact of El Niño on Australian rainfall using available observations from the postsatellite era. Of particular interest is the difference in impact between classical El Niño events wherein peak sea surface temperature (SST) anomalies appear in the eastern Pacific and the recently termed El Niño ''Modoki'' events that are characterized by distinct warm SST anomalies in the central Pacific and weaker cold anomalies in the west and east of the basin. A clear interseasonal and interevent difference is apparent, with the maximum rainfall response for Modoki events occurring in austral autumn compared to austral spring for classical El Niños. Most interestingly, the Modoki and non-Modoki El Niño events exhibit a marked difference in rainfall impact over Australia: while classical El Niños are associated with a significant reduction in rainfall over northeastern and southeastern Australia, Modoki events appear to drive a large-scale decrease in rainfall over northwestern and northern Australia. In addition, rainfall variations during March–April–May are more sensitive to the Modoki SST anomaly pattern than the conventional El Niño anomalies to the east.

1. Introduction

Australia generally experiences below-average rain during El Niño events. This relationship is thought to be modulated by interdecadal variations in Pacific Ocean sea surface temperature (SST; e.g., Nicholls et al. 1996; Power et al. 1999; Arblaster et al. 2002; Suppiah 2004). One of the largest recorded El Niño events occurred in 1997/98, yet this had only a modest impact on Australian rainfall. In contrast, severe drought in Australia resulted from the weak 2002/03 El Niño event. Curiously, both events occurred at the same phase of the so-called Interdecadal Pacific Oscillation (Power et al. 1999), suggesting that much of the relationship between the El Niño–Southern Oscillation (ENSO) and Australian rainfall remains poorly understood. Recently, Wang and Hendon (2007) attempted to clarify this paradigm by showing that warm SST anomalies were located in the eastern Pacific during 1997 and in the central west during 2002, suggesting that Australian rainfall is sensitive to the zonal distribution of SST anomalies along the tropical Pacific during ENSO events.

The leading mode of an empirical orthogonal function (EOF) analysis performed with Pacific Ocean SST yields the well-known El Niño pattern with peak SST anomalies in the eastern Pacific (e.g., Rasmusson and Carpenter 1982; Trenberth 1997). This mode accounts for approximately half the total variance of Pacific Ocean SST, depending on the dataset used and the period analyzed. For example, Ashok et al. (2007) obtained 45% of total variance in the classical El Niño mode using the Hadley Centre Sea Ice and Sea Surface Temperature dataset (HadISST; Rayner et al. 2003) from the period 1979–2004, while Wang and Hendon (2007) found 51% for the leading mode using the September–November (SON) time series derived from Reynolds and Smith (1994).

Recent studies have shown that the second mode of Pacific Ocean variability is represented by warm anomalies in SST located in the central Pacific, accounting for approximately 12% of total variance (e.g., Wang and Hendon 2007; Ashok et al. 2007). This mode, recently referred to as the El Niño ''Modoki'' (Ashok et al. 2007), is characterized by warm central Pacific waters and cool SST anomalies on both the eastern and western regions of the basin. The El Niño Modoki mode

Corresponding author address: Andréa S. Taschetto, Climate Change Research Centre, University of New South Wales, Sydney, NSW 2052, Australia.
E-mail: a.taschetto@unsw.edu.au

DOI: 10.1175/2008JCLI2589.1

has been proposed as independent of the traditional ENSO (Ashok et al. 2007; Weng et al. 2007). Yet the mechanisms driving this mode of variability in the Pacific Ocean remain unclear. Ashok et al. (2007) suggest that the recent weakening of equatorial easterlies in the central Pacific, and the enhanced easterlies to the east, has weakened the zonal gradient of SST and flattened the thermocline, leading to a climate state that favors more frequent Modoki events. The authors describe an associated tripolar sea level pressure anomaly pattern during the Modoki evolution, and they report the presence of two anomalous Walker circulation cells in the troposphere instead of the single cell pattern associated with the typical El Niño mode. The joint ascending branch of this double Walker circulation is located over the central equatorial Pacific, and the western descending branch is located over Indonesia and northern Australia. This configuration seems to influence regional climate in a different way than conventional El Niños. For example, Weng et al. (2007) use three Modoki events to estimate its climate impact over Japan, China, and the United States during boreal summer [June–August (JJA)]. They show that the El Niño Modoki event tends to dry areas that normally experience wet or normal conditions during a traditional El Niño event.

One of the key goals of this study is to extend the Weng et al. (2007) analysis to focus on the Australian region. In addition, we use a singular value decomposition (SVD) analysis and composite statistics to assess the impacts of the traditional El Niño and the El Niño Modoki pattern on Australian rainfall. While previous studies tend to concentrate on austral winter (JJA), we focus on the rainfall impacts during austral autumn [March–May (MAM)], a season that we will show to be characterized by the maximum El Niño Modoki–induced anomalies in rainfall over Australia. The main goal of this note is simply to identify the different areas of Australia most impacted by El Niño and El Niño Modoki events, with only limited analysis of the associated atmospheric dynamics. The rest of this note is divided as follows: the datasets and methods are described in section 2, the results are discussed in section 3, and the major conclusions are summarized in section 4.

2. Data and methods

The datasets used in this study include the global sea ice and sea surface temperature analyses from the Hadley Centre (HadISST1) (Rayner et al. 2003). The HadISST1 data have a spatial resolution of 1° latitude × 1° longitude and have been shown to be an improvement upon the Global Sea Ice coverage and SST (GISST) dataset (Rayner et al. 2003). Monthly precipitation data are based on the high-quality daily rainfall data from the Australian Bureau of Meteorology (Lavery et al. 1992). This dataset is displayed on a regular 0.5° grid covering Australia from 10° to 44°S and 112° to 154°E. Atmospheric vertical velocity and velocity potential from the National Centers for Environmental Prediction–National Center for Atmospheric Research (NCEP–NCAR) reanalysis are also employed in this study (Kistler et al. 2001). The datasets cover the period 1979–2004.

SVD analyses are used to show the coupled spatial patterns between the SST anomalies in the tropical Pacific Ocean and rainfall anomalies over Australia. The SVD method is a generalization of the EOF analysis, using two combined data fields. To identify pairs of coupled patterns between two fields, the SVD analysis performs a singular value decomposition of the cross-covariance matrix between two space- and time-dependent data fields. The result is a spatially orthogonal set of singular vectors (analogous to the eigenvectors in the EOF) and a set of singular values associated with each pair of vectors (analogous to EOF eigenvalues) that explain some quantifiable fraction of the squared covariance between the two fields. As in the EOF analysis, the time series of expansion coefficients is determined by projecting the original field onto the singular vectors. For more details of the SVD method for climate applications see Bjornsson and Venegas (1997).

Apart from SVD analyses, we also consider composite statistics of Pacific Ocean SST, Australian rainfall, velocity potential, and vertical velocity during classical El Niño and El Niño Modoki events. The choice of years is determined by examination of the associated Pacific Ocean SST anomalies during the season of interest. The years from the postsatellite era used to characterize traditional El Niño events, focused on the September–October–November season are 1982, 1987, and 1997. For comparison, we composite the El Niño Modoki events of 1980, 1987, 1991, 1995, and 2003, this time focused on the austral autumn season (March–May). The selected years are in broad agreement with classical El Niños as defined by Trenberth (1997) and the Modoki events identified by Ashok et al. (2007). Significance levels of the composite anomaly patterns are calculated using a two-tailed Student's t test. In general, throughout this paper, the datasets are analyzed for the austral seasons, namely, MAM for autumn and SON for spring.

3. Results

An SVD analysis performed on the complete 1979–2006 monthly anomaly time series of tropical Pacific SST and rainfall over Australia reveals the traditional

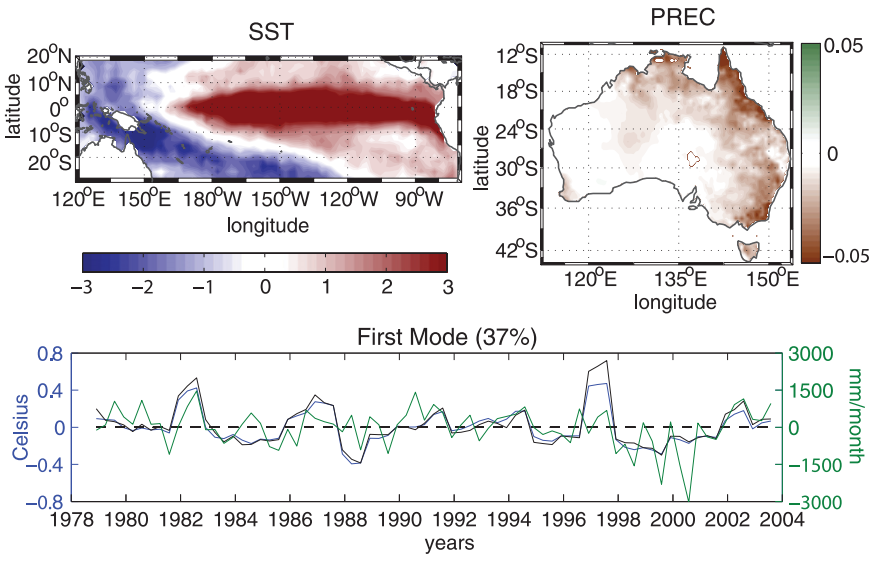

FIG. 1. (top) Leading mode of SVD analysis between (left) SST in the tropical Pacific and (right) Australian rainfall during SON. (bottom) Time series of the SVD expansion coefficient. Blue line: the SST mode (°C). Green line: the rainfall mode (mm month^{-1}). Black line: Niño-3 index scaled by 0.2. The correlation coefficient between the SST and rainfall time series is 0.50 and between Niño-3 and SST is 0.98.

El Niño patterns (figure not shown), namely, maximum SST anomalies over the eastern Pacific and maximum rainfall reduction over eastern Australia. This rainfall anomaly pattern is also apparent in correlation analyses between the Southern Oscillation index (SOI; or indeed other Niño indexes) and Australian rainfall, as reported in previous studies (e.g., McBride and Nicholls 1983; Ropelewski and Halpert 1989; Drosdowsky and Williams 1993). However, El Niño events tend to peak during late spring and terminate February–March (Trenberth 1997). Therefore, stratifying ENSO analyses by season is important. In particular, consistent rainfall correlations are found over eastern Australia beginning in winter and extending through to the following summer (Drosdowsky and Williams 1993). We therefore first focus our analyses on the austral spring season (SON) when Australian rainfall variations seem most susceptible to El Niño (McBride and Nicholls 1983).

Figure 1 shows the dominant coupled mode of variability between Pacific SST anomalies and Australian rainfall during SON. The SST mode of variability during SON shows a clear warm anomaly across the equator, extending from the central to the eastern Pacific, and cool anomalies in the west, representing the traditional El Niño structure. This pattern is accompanied by negative anomalies of precipitation over Australia, consistent with Ropelewski and Halpert (1987) and Drosdowsky and Williams (1993). This strong coupling between the El Niño phenomenon and reduced rainfall over Australia is responsible for 37% of the square covariance fraction. The associated time series of SST and rainfall exhibits a correlation coefficient of 0.50, significant at the 95% level. The time series associated with the SST mode is highly significantly correlated with the Niño-3 index, with a coefficient of 0.98.

When the SVD analysis is now carried out during austral autumn (MAM), the leading mode of variability shows markedly different SST and rainfall anomaly patterns (Fig. 2). In particular, anomalously warm waters are now located in the central to western Pacific, with cool tropical anomalies located on either side to the east and west. This SST pattern matches the El Niño Modoki of Ashok et al. (2007), who use an EOF analysis of all *monthly* tropical Pacific SST anomalies to show that these events are revealed in the second mode, explaining 12% of the total variance. Figure 2 reveals that the leading mode of SVD analysis of SST and rainfall during the MAM season accounts for 25% of the square covariance fraction. This suggests that during MAM the Modoki pattern is more important for Australian rainfall variations than the traditional ENSO signal. It is interesting to note that only for the MAM season does the Modoki SST pattern appear as the first SVD coupled mode. The strong coupling between SST and the rainfall mode in MAM (Fig. 2) is indicated by a significant correlation of 0.53 between the time series of expansion coefficients of both variables. This mode of variability is associated with different rainfall anomalies over Australia; namely, the northern and northwestern regions now see significant reductions. The time series

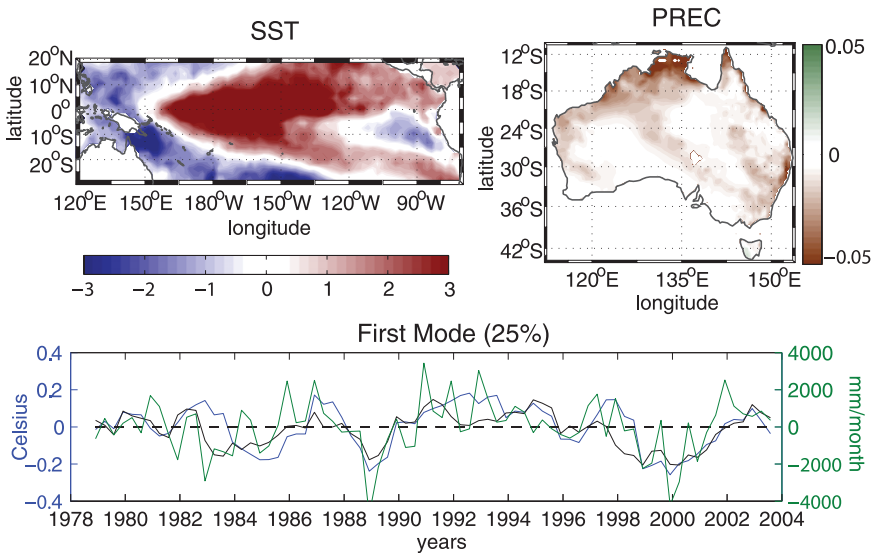

FIG. 2. As in Fig. 1, but for MAM. Black line: El Niño Modoki index (EMI) scaled by 0.2. The correlation coefficient between the SST and rainfall time series is 0.53 and between the EMI and SST is 0.69.

of expansion coefficients for the SST is significantly correlated (0.69 coefficient) with the El Niño Modoki index as defined by Ashok et al. (2007).

To assess the robustness of the SVD analysis we also analyze composite fields of SST, precipitation, vertical velocity, and velocity potential for ENSO and El Niño Modoki events. Figure 3 shows the composite anomaly patterns for each of these variables for the SON phases of ENSO during 1982, 1987, and 1997 (Fig. 3a, left column) and the Modoki-like phases during MAM in 1980, 1987, 1991, 1995, and 2003 (Fig. 3b, right column). The El Niño composite shows strong positive SST anomalies extending from the South American coast to the central Pacific, accompanied by anomalous upward motion throughout the troposphere between 180°E and 90°W, and an intensified upward flux at 150°W. Anomalous divergence is seen over the tropical Pacific and consequent descending motion is located over the Indonesian region and Australia, demonstrating the well-known displacement of the Walker circulation during ENSO years. Rainfall anomalies are weak over much of the continent, with a limited area of significant decrease in the southeast. It is important to note, however, that the rainfall composite is weak because only three events are averaged and, of these, the 1997 ENSO event actually saw modest increases in SON rainfall over significant parts of eastern Australia, offsetting the other two events. When the period 1950–2003 is considered, the rainfall composite for all post-1950 ENSO events reveals a clearer reduction in precipitation over eastern Australia (see Fig. 4).

The Modoki SST composite in MAM (Fig. 3, right panel) is very similar to the first SVD mode shown in Fig. 2, demonstrating the robustness of this SST pattern. The corresponding MAM rainfall composites exhibit below-average rainfall across significant areas of Australia, particularly the north and northwest.

The composite of Modoki vertical velocity (Fig. 3, right panel) shows an upward motion through the deep troposphere centered at 180°W, shifted westward when compared to the rising air in the conventional ENSO-composite circulation. The distribution of velocity potential at 200 hPa also confirms anomalous divergence shifted slightly to the west in the central Pacific as a consequence of ascending air over the warm central Pacific SST anomalies. The anomalous divergence in the central-west Pacific causes convergence and thus subsidence over South America and the Indonesian region. This can also be seen in the standard El Niño composites, although with different magnitudes and with regions of ascent–descent generally shifted to the east compared to Modoki. Interestingly, the descending air anomaly over northwestern Australia is stronger in the standard El Niño during SON compared to the Modoki El Niño during MAM, even though greater rainfall impacts are seen during the Modoki events. Nevertheless, subsidence is still apparent from the high–midtroposphere, suggesting a reduction in deep convection processes. An analysis of the vertical velocity anomalies averaged over the Australian longitudes (5°–15°S, figure not shown) reveals slightly stronger subsidence throughout the troposphere when compared to the composite averaged over

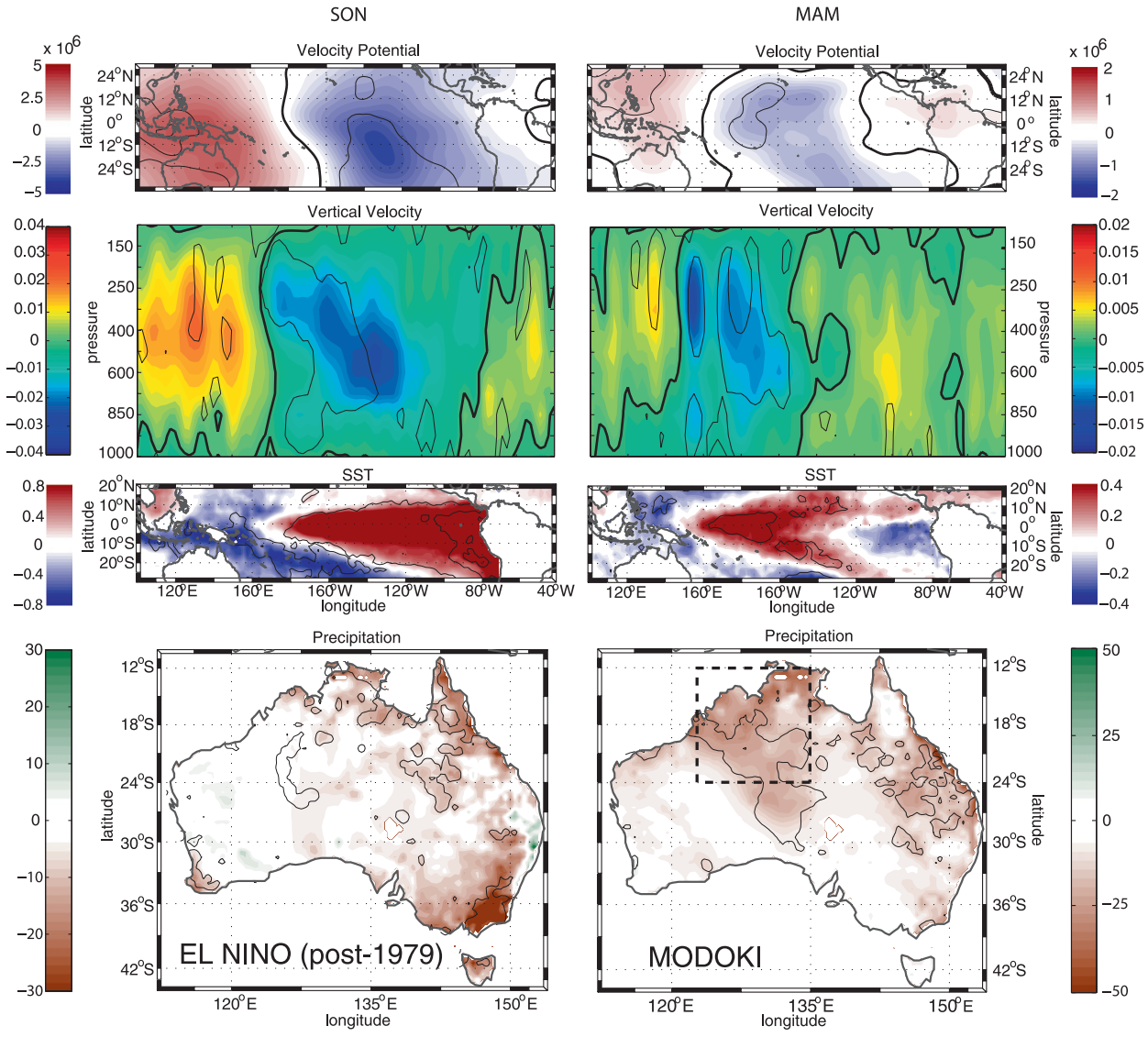

FIG. 3. Composites of (top to bottom) velocity potential at 200 hPa in $m^2\ s^{-1}$, vertical velocity in Pa s^{-1} averaged over 10°N–10°S, SST in °C, and precipitation in mm $month^{-1}$ during (left) SON for ENSO: 1982, 1987, and 1997 and (right) MAM for the El Niño Modoki: 1980, 1987, 1991, 1995, and 2003. Areas within the thin black lines are significant at the 90% confidence level using the Student's *t* test. The thick black contours in the velocity potential and vertical velocity panels represent the zero line. (bottom right) The area within the black dashed box is averaged to create the rainfall time series used in Figs. 5 and 6.

10°N–10°S. It is important to note, however, that a relatively weak subsidence over Northern Australia may impact net MAM rainfall more strongly than during SON, as the austral autumn season receives climatologically more rainfall than austral spring over the region. The stronger descent over Indonesia in El Niño than in Modoki was also observed by Weng et al. (2007). On the other hand, the subsidence over the east is weaker in ENSO than in Modoki events. The dynamical consequence of the ascending circulation over the central Pacific is two branches of anomalous subsidence over the eastern and western Pacific, consistent with Ashok et al. (2007), who demonstrate a different atmospheric response to the SST anomalies associated with El Niño Modoki when compared to traditional ENSO events. A tripole structure of the upper-level divergence–convergence occurs over the tropical Pacific, leading to an anomalous two-cell Walker circulation, the heart of the El Niño Modoki phenomenon according to Ashok et al. (2007).

4. Discussion and conclusions

In this study we have demonstrated that Australian rainfall is sensitive to varying El Niño SST anomalies

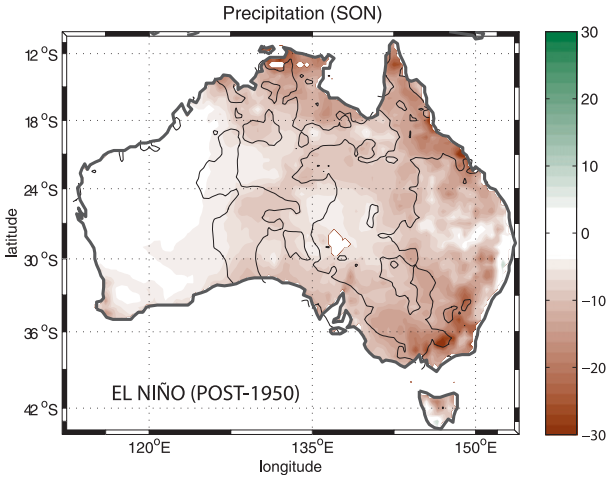

FIG. 4. Composite of precipitation anomalies (mm month^{-1}) for ENSO during the SON season from 1950 to 2004 (i.e., 1951, 1957, 1963, 1965, 1968, 1969, 1972, 1982, 1987, and 1997). Areas within thin black lines are significant at the 95% confidence level using a Student's *t* test.

over the Pacific Ocean. In particular, the location of anomalously low rainfall appears to be sensitive to the zonal position of maximum SST anomalies along the equatorial Pacific. While traditional El Niño events cause reduced rainfall over northeastern and southeastern Australia, the Modoki configuration tends to influence rainfall over the north and northwest of Australia. Furthermore, the period of maximum impact of traditional El Niño (September–November) and El Niño Modoki (March–May) varies by more than one season. During the Modoki events, warm equatorial SST anomalies induce rising air over the central-west Pacific and subsidence over northwestern Australia. As a consequence of this anomalous descending air, rainfall is reduced in the region with strongest impact during MAM.

It is interesting to note that during the period 1979–2003 there have been more El Niño Modoki events than traditional El Niños, suggesting a late-twentieth-century tendency toward a warmer central Pacific compared to the eastern Pacific. This could be one of the factors forcing the post-1970s reduction in rainfall over northern Australia during the austral autumn season (Taschetto and England 2008). Another interesting feature related to the Modoki index is the long-term variability presented in the time series of Fig. 2, which sees a larger number of Modoki events concentrated in the early-1990s. This decadal variability in the Modoki index has also been observed by Ashok et al. (2007).

Whether the El Niño Modoki is an independent climate mode or just a variation on the traditional ENSO is not the focus of this study. Because the time series of the two SVD expansion coefficients exhibit similarities and as the Modoki SST anomalies peak one season later than the traditional El Niño, it is quite possible that the Modoki simply represents a late phase of the El Niño cycle. Regardless of this, we have shown that the Modoki SST is associated with markedly different Australian rainfall anomalies compared to the standard El Niño, with a greater impact over northern and northwestern Australia.

There remain several unanswered questions as to the dynamical framework of the El Niño Modoki–Australian rainfall linkages found in this study. First, why do Modoki-like SST anomalies produce the maximum rainfall response over northern and northwestern Australia during MAM rather than during December–February (DJF) when the Modoki event is thought to be stronger? Second, why do the Modoki events appear to drive a weaker anomalous circulation over Australia compared to ENSO, despite generating larger impacts on regional rainfall? This latter fact, as stated above, could simply be symptomatic of the larger mean MAM rainfall compared to the SON season.

Given the weaker atmospheric circulation anomalies and yet the marked northern Australian rainfall response during MAM for the Modoki events, it is plausible that the mechanisms involve an oceanic teleconnection between the tropical Pacific and the Indonesian–western Indian Ocean regions. Previous studies have reported a linkage between ENSO and the Indian Ocean Dipole (IOD) via the Indonesian Throughflow (e.g., Clarke 1991; Clarke and Liu 1994; Meyers 1996; Potemra 2001; Cai et al. 2005). For example, Meyers (1996) and England and Huang (2005) observe that the volume transport of the Indonesian Throughflow varies during the ENSO cycle. Cai et al. (2005) find a similar relationship, noting that the observed SST anomalies off Western Australia reach a maximum approximately 3 months after the El Niño peak, via propagating Rossby and Kelvin waves. The anomalies in the western Indian Ocean can trigger an IOD event in the ensuing months (e.g., Saji et al. 1999; Saji and Yamagata 2003).

It is well known that the IOD affects rainfall over southern regions of Australia during late winter and early spring, when the IOD mode is at its mature phase (Ashok et al. 2003; Ummenhofer et al. 2009). As IOD events are strongly seasonally phase locked, their impacts on Australian rainfall during DJF and MAM have not been identified. To assess the relative influence of the Indian and Pacific Oceans on northern Australian rainfall, a lagged correlation analysis is performed (Fig. 5) between SST anomalies and the time series of northern Australia MAM rainfall averaged over 24°–12°S, 125°–135°E. Figure 5 reveals the evolution of the Pacific Ocean SST anomalies from DJF to MAM

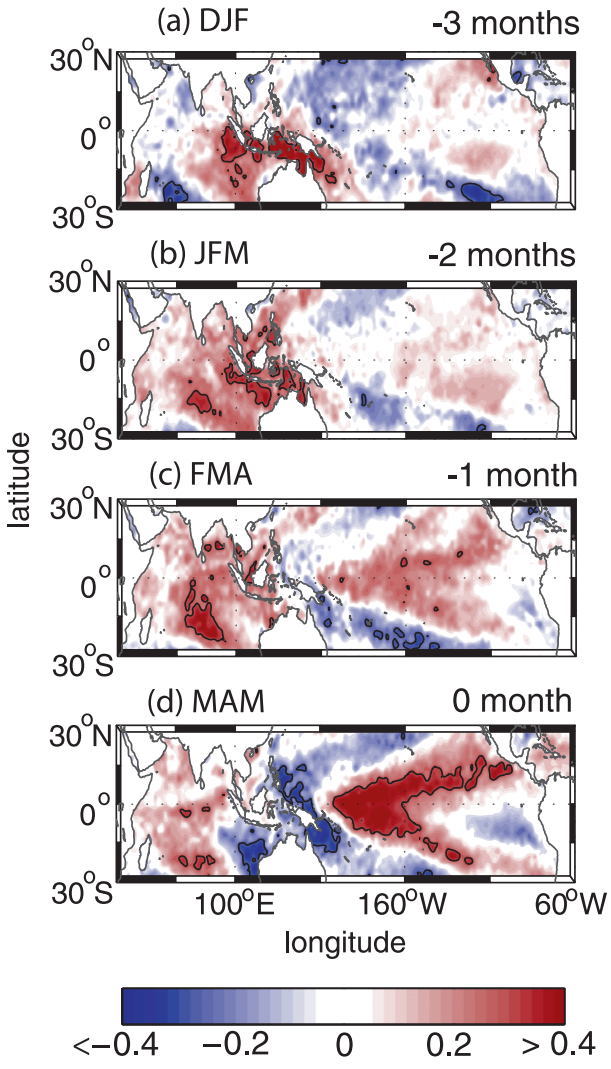

FIG. 5. Lagged correlation analysis between the time series of northern Australian MAM rainfall averaged over 24°–12°S, 125°–135°E and Pacific–Indian Ocean SST anomalies. Areas within the thin black lines are significant at the 95% confidence level using a Student's *t* test. The precipitation time series is sign reversed before analysis for comparison with Figs. 2 and 3.

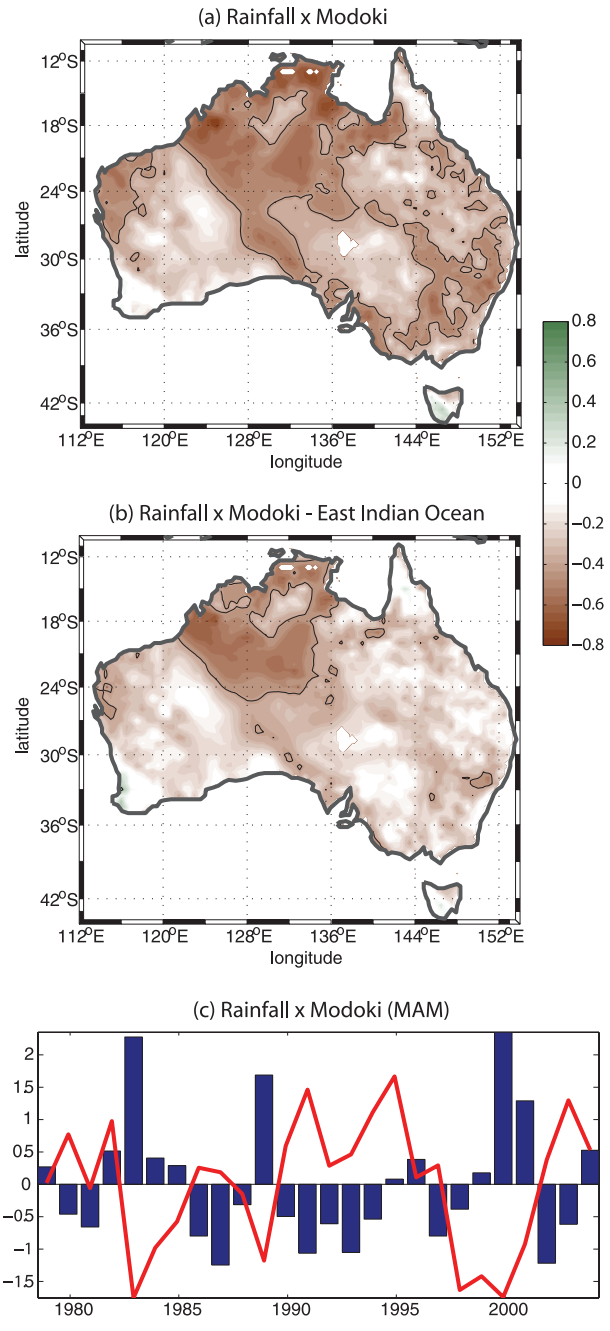

FIG. 6. (a) Correlation analysis between rainfall and the Modoki index in MAM. (b) Same as (a), but excluding the effect of eastern Indian Ocean SST anomalies via a partial correlation analysis. Areas within the thin black lines are significant at the 95% confidence level using a Student's *t* test. (c) Standardized time series of MAM rainfall in the averaged area shown in Fig. 3 (blue bars) and the Modoki index (red line) during 1979–2004.

(at 1-month increments) when a Modoki-like SST pattern is established, with the maximum rainfall response. During MAM, the season of peak rainfall response, positive correlation coefficients off Western Australia are seen, suggesting a possible teleconnection from the Modoki peak SST anomaly region to the eastern Indian Ocean, as reported by previous studies. Note, however, that this SST pattern is not a conventional IOD signature, with the cold pole displaced to the south.

Correlations between northern Australian rainfall and the IOD index do not show significant values, except when the analysis is performed only with the eastern Indian Ocean anomalies, a region thought to be important for precipitation across the country (e.g., Ummenhofer et al. 2008). Nevertheless, a partial correlation analysis applied between the Modoki index and Australian rainfall, after removing the effect of SST

anomalies off Western Australia (15°–20°S, 110°–125°E), yields a significant and consistent correlation pattern over northern/northwestern Australia (cf. Figs. 6a and 6b). The relationship between Australian rainfall and the Modoki SST mode is also shown in Fig. 6c, which presents a clear anticorrelated pattern of variability between the time series of precipitation averaged in the northern region and the Modoki index in MAM. These simple analyses suggest that the Modoki SST pattern plays a greater role in drying northern Australia during MAM than the western Indian Ocean anomalies. In contrast, the correlation pattern over southeastern Australia is significantly reduced (Fig. 6b), indicating an Indian Ocean SST signature in that region. A similar partial correlation analysis for the SON season of the canonical ENSO mode reveals an IOD influence over southeastern Australia (figure not shown). To a large extent the observational data record is too short to properly address these questions. Instead, these issues will be addressed in a future study employing coupled and atmospheric general circulation models with El Niño Modoki SST anomalies applied over the tropical Pacific Ocean.

Acknowledgments. This work was supported by the Australian Research Council. The authors thank Caroline Ummenhofer, Alex Sen Gupta, and the anonymous reviewers for helpful comments and discussions.

REFERENCES

Arblaster, J. M., G. A. Meehl, and A. M. Moore, 2002: Interdecadal modulation of Australian rainfall. *Climate Dyn.,* **18,** 519–531.

Ashok, K., Z. Guan, and T. Yamagata, 2003: Influence of the Indian Ocean dipole on the Australian winter rainfall. *Geophys. Res. Lett.,* **30,** 1821, doi:10.1029/2003GL017926.

——, S. K. Behera, S. A. Rao, H. Weng, and T. Yamagata, 2007: El Niño Modoki and its possible teleconnection. *J. Geophys. Res.,* **112,** C11007, doi:10.1029/2006JC003798.

Bjornsson, H., and S. A. Venegas, 1997: A manual for EOF and SVD analyses of climate data. CCGCR Rep. 97–1, McGill University, Montréal, QC, Canada, 52 pp.

Cai, W., G. Meyers, and G. Shi, 2005: Transmission of ENSO signal to the Indian Ocean. *Geophys. Res. Lett.,* **32,** L05616, doi:10.1029/2004GL021736.

Clarke, A. J., 1991: On the reflection and transmission of low-frequency energy at the irregular western Pacific Ocean boundary. *J. Geophys. Res.,* **96,** 3289–3305.

——, and X. Liu, 1994: Interannual sea level in the northern and eastern Indian Ocean. *J. Phys. Oceanogr.,* **24,** 1224–1235.

Drosdowsky, W., and M. Williams, 1993: The Southern Oscillation in the Australian region. Part I: Anomalies at the extremes of the oscillation. *Int. J. Climatol.,* **13,** 111–149.

England, M. H., and F. Huang, 2005: On the interannual variability of the Indonesian Throughflow and its linkage with ENSO. *J. Climate,* **18,** 1435–1444.

Kistler, R., and Coauthors, 2001: The NCEP–NCAR 50-Year Reanalysis: Monthly means CD-ROM and documentation. *Bull. Amer. Meteor. Soc.,* **82,** 247–267.

Lavery, B., A. Kariko, and N. Nicholls, 1992: A historical rainfall data set for Australia. *Aust. Meteor. Mag.,* **40,** 33–39.

McBride, J. L., and N. Nicholls, 1983: Seasonal relationships between Australian rainfall and the Southern Oscillation. *Mon. Wea. Rev.,* **111,** 1998–2004.

Meyers, G., 1996: Variation of the Indonesian throughflow and the El Niño–Southern Oscillation. *J. Geophys. Res.,* **101,** 12 255–12 263.

Nicholls, N., B. Lavery, C. Frederiksen, W. Drosdowsky, and S. Torok, 1996: Recent changes in relationships between the El Niño–Southern Oscillation and Australian rainfall and temperature. *Geophys. Res. Lett.,* **23,** 3357–3360.

Potemra, J. T., 2001: Contribution of equatorial Pacific winds to southern tropical Indian Ocean Rossby waves. *J. Geophys. Res.,* **106,** 2407–2422.

Power, S., T. Casey, C. Folland, A. Colman, and V. Mehta, 1999: Interdecadal modulation of the impact of ENSO on Australia. *Climate Dyn.,* **15,** 319–324.

Rasmusson, E. M., and T. H. Carpenter, 1982: Variations in tropical sea surface temperature and surface wind fields associated with the Southern Oscillation/El Niño. *Mon. Wea. Rev.,* **110,** 354–384.

Rayner, N. A., D. E. Parker, E. B. Horton, C. K. Folland, L. V. Alexander, D. P. Rowell, E. C. Kent, and A. Kaplan, 2003: Global analyses of SST, sea ice and night marine air temperature since the late nineteenth century. *J. Geophys. Res.,* **108,** 4407, doi:10.1029/2002JD002670.

Reynolds, R., and T. Smith, 1994: Improved global sea surface temperature analyses using optimum interpolation. *J. Climate,* **7,** 929–948.

Ropelewski, C. F., and M. S. Halpert, 1987: Global and regional scale precipitation patterns associated with the El Niño/Southern Oscillation. *Mon. Wea. Rev.,* **115,** 1606–1626.

——, and ——, 1989: Precipitation patterns associated with the high index phase of the Southern Oscillation. *J. Climate,* **2,** 268–284.

Saji, N. H., and T. Yamagata, 2003: Structure of SST and surface wind variability during Indian Ocean dipole mode events: COADS observations. *J. Climate,* **16,** 2735–2751.

——, B. N. Goswami, P. N. Vinayachandran, and T. Yamagata, 1999: A dipole mode in the tropical Indian Ocean. *Nature,* **401,** 360–363.

Suppiah, R., 2004: Trends in the Southern Oscillation phenomenon and Australian rainfall and changes in their relationship. *Int. J. Climatol.,* **24,** 269–290.

Taschetto, A. S., and M. H. England, 2008: An analysis of late 20th Century trends in Australian rainfall. *Int. J. Climatol.,* **29,** 791–807, doi:10.1002/joc.1736.

Trenberth, K. E., 1997: The definition of El Niño. *Bull. Amer. Meteor. Soc.,* **78,** 2771–2777.

Ummenhofer, C. C., A. Sen Gupta, M. J. Pook, and M. H. England, 2008: Anomalous rainfall over southwest Western Australia forced by Indian Ocean sea surface temperatures. *J. Climate,* **21,** 5113–5134.

——, M. H. England, P. C. McIntosh, G. A. Meyers, M. J. Pook, J. S. Risbey, A. Sen Gupta, and A. S. Taschetto, 2009: What causes Southeast Australia's worst droughts? *Geophys. Res. Lett.,* **36,** L04706, doi:10.1029/2008GL036801.

Wang, G., and H. H. Hendon, 2007: Sensitivity of Australian rainfall to inter–El Niño variations. *J. Climate,* **20,** 4211–4226.

Weng, H., K. Ashok, S. K. Behera, S. A. Rao, and T. Yamagata, 2007: Impacts of recent El Niño Modoki on dry/wet conditions in the Pacific rim during boreal summer. *Climate Dyn.,* **29,** 113–129.